

Statistical and machine learning ensemble modelling to forecast sea surface temperature

Stefan Wolff^a, Fearghal O'Donncha^{b,*}, Bei Chen^b

^a*PI, University of Bonn - Germany, Bonn*
^b*IBM Research - Ireland, Dublin*

Abstract

In situ and remotely sensed observations have huge potential to develop data-driven predictive models for oceanography. A suite of machine learning models, including regression, decision tree and deep learning approaches were developed to estimate sea surface temperatures (SST). Training data consisted of satellite-derived SST and atmospheric data from The Weather Company. Models were evaluated in terms of accuracy and computational complexity. Predictive skills were assessed against observations and a state-of-the-art, physics-based model from the European Centre for Medium Weather Forecasting. Results demonstrated that by combining automated feature engineering with machine-learning approaches, accuracy comparable to existing state-of-the-art can be achieved. Models captured seasonal trends in the data together with short-term variations driven by atmospheric forcing. Further, it demonstrated that machine-learning-based approaches can be used as transportable prediction tools for ocean variables – a challenge for existing physics-based approaches that rely heavily on user parametrisation to specific geography and topography. The low computational cost of inference makes the approach particularly attractive for edge-based computing where predictive models could be deployed on low-power devices in the marine environment.

Keywords: machine learning, sea surface temperature, forecasting, modelling, statistical models

1. Introduction

Sea surface temperature (SST) is a common indicator of primary productivity in aquaculture [1], critical for operation of marine-based industries such as power plants [2], while being central to better understanding interactions between the ocean and the atmosphere [3]. Recent decades has seen enormous progress in approaches to sample SST. In particular, satellite technology has vastly increased the granularity of measurements that are possible, providing long-term global measurements at varying spatial and temporal resolution. MODIS (or Moderate Resolution Imaging Spectroradiometer) is a key instrument aboard the Terra and Aqua satellites, which acquire imagery data for 36 spectral bands, from which information on a range of oceanic processes, including SST, can be extracted.

Concurrently, improvements in high-resolution ocean models together with increased computational capabilities have made sophisticated data-assimilation (DA)

schemes feasible – leading to a number of reanalysis products that provide accurate forecasts across broad spatial and temporal scales. Reanalyses yield numerical estimates of the true ocean state by combining models with observations to improve short-term predictions by providing more representative initial conditions. A state-of-the-art reanalysis is the ERA5 global dataset from the European Centre for Medium-Range Weather Forecasts (ECMWF) [4]. It provides short-term SST forecasts (and hindcasts) on a 32 km horizontal grid at hourly intervals from a numerical synthesis of ocean models, atmospheric forcing fluxes, and SST measurements.

These analysis and forecasting systems face a number of scientific, technical, and practical challenges.

- The computational and operational requirements for ocean simulations at appropriate scales are immense and require high performance computing (HPC) facilities to provide forecasts and services in practical time frames [5].
- Operational forecasting systems require robust data assimilation schemes that takes account of biases and errors in models and observations [6].

*Corresponding author

Email address: feardonn@ie.ibm.com (Fearghal O'Donncha)

Proposed assimilation schemes consider a wide variety of approaches to account for different error sources broadly decomposed across *a-priori* based approaches that incorporate information on physical relationship between variables and *statistical* approaches that are typically based on ensemble model projections [7]. A consequence of these challenges is that operational forecasting systems are only feasible for large research centres or collaborations who have access to large-scale compute resources and scientific expertise.

An alternative approach is to leverage the large datasets generated by ocean monitoring and modelling tools to train machine-learning-based forecasting models. Once trained, the computational expense of these products are negligible, and conceptually, one can develop transportable models that can be trained to learn features at different geographical location. This paper presents a suite of data-driven modelling approaches for developing robust systems to predict sea-surface temperature (SST). An automatic feature-engineering module was implemented to identify the key features at disparate geographical locations to provide a transportable forecasting system. Finally, the different models were averaged using a model-scoring and weighting approach to provide an ensemble prediction that outperformed the best-performing individual model. Contributions are as follows:

- We evaluated the predictive skill of a range of data-driven modelling approaches from the perspective of (1) balancing computational complexity with predictive skill and (2) leveraging ensemble aggregation to improve robustness.
- We developed an autonomous feature-engineering module to (1) improve the portability of the model to different geographical locations and (2) reduce the appetite for training data by providing a more intelligent supply of explanatory variables.
- Finally, we assessed performance of the modelling framework globally, against a state-of-the-art physics-based model.

While the idea of using ML to provide computationally cheaper surrogate models has been previously explored, the distinctive characteristics of SST lie in their complex temporal dependence structure and multi-level seasonality. To our knowledge, this application has not yet been considered in the existing literature. We demonstrate the viability of the approach to capture the short- and long-term trends: integrating different ML based models with different temporal performance characteris-

tics in an ensemble approach provides accuracy on par with large scale complex models.

In the next section, we discuss prior research in the domain. Subsequently, the different models are introduced along with the feature extraction and ensemble aggregation techniques. Section 4 compares performances of the different models along with the predictive accuracy of individual and ensemble aggregated models. The portability of the system to different geographical locations is discussed. Finally, we present conclusions from the research and discuss future work.

2. Related Work

A wide variety of operational SST forecasting products exist that leverage physics-based circulation modelling and data assimilation to resolve temperature distributions. A representative example is the forecasting system for the North-West Atlantic from the NEMO Community Ocean Model, which provides a variety of ocean variables at 12 km resolution. Inputs to the system include: lateral boundary conditions from the open-ocean supplied by a (coarser) global model, atmospheric fluxes from the Met Office Unified Model and river inputs from 320 European rivers [8]. Other examples include the National Centers for Environmental Prediction Climate Forecast System, which provides global predictions of SST at 110 km resolution [9], and the US Navy HYCOM Global Forecasting System, which provides 5-day forecasts at resolution ranging from 4–20 km [10] together with localised, regional models at higher resolution [11, 12]. The common feature of these modelling systems is the high computational demands that generally limit either the precision (coarse global models) or the size of the domain (high-resolution, regional models).

Due to the heavy computational overhead of physical models, there is an increasing trend to apply data-driven deep-learning (DL) / machine-learning (ML) methods to model physical phenomena [13, 14]. Application of ML-based approaches has been categorised into three areas [15]:

1. The system’s deterministic model is computationally expensive and ML can be used as a code accelerator.
2. There is no deterministic model but an empirical ML-based model can be derived using existing data.
3. Classification problems.

A number of studies have investigated data-driven approaches to provide computationally cheaper surrogate

models, applied to such things as wave forecasting [16], viscoelastic earthquake simulation [17], and water-quality investigation [18]. ML based approaches have been considered to spatially interpolate environmental variables and improve precision of solution [19]. DL-based approaches have been adopted to increase the resolution of satellite imagery through down-scaling techniques [20]. A number of studies have presented data-mining approaches that extract pertinent events from measured data such as detection of harmful algal blooms [21].

Distinctive characteristics of SST are their complex temporal-dependence structure and multi-level seasonality. There are only a few options to describe systems with such characteristics, including: (1) Generalized Additive Models (GAMs) from classic statistics, (2) Random Forest (RF) and extreme gradient boosting (XGBoost) from ML, and (3) Multi-Layer Perceptron (MLP) and Long Short-Term Memory (LSTM) models from DL, which are all considered in this paper.

3. Methodology

Training data for this study were from the MODIS instrument aboard the NASA *Aqua* satellite. MODIS SSTs are produced and made available to the public by the NASA GFSC Ocean Biology Processing Group. The MODIS sensor measures ocean temperature (along with other ocean products such as salinity and Chlorophyll concentration) from a layer less than 1 mm thick at the sea surface. Data are available from 2002 to present at 4 km horizontal resolution and daily intervals. Calibration of the Pathfinder algorithm coefficients and tuning of instrument configurations produce accurate measurements of SST with mean squared error (MSE) against *in situ* sensors $< 0.2^\circ\text{C}$ [22]. These accurate global SST measurement on decadal periods, serve as an ideal dataset to extract insights using ML. Atmospheric variables also serve as features to the models and were extracted at 30-km spacing from The Weather Company (TWC).

3.1. Prediction Models

The selected models, namely, GAM, RF, XGBoost, MLP, and LSTM, were assessed in terms of accuracy and computational complexity. The objective of each was to relate a univariate response variable y to a set of explanatory variables $\mathbf{x} = x_1, x_2, \dots, x_i$ (representing for example, historical SST, air temperature, seasonal identifier, etc.).

GAM-based models characterize general nonlinear regressions without requiring pre-specification of the

form of the nonlinear relationship. Predicting y from the vector of covariates \mathbf{x} , at time t is as [23]:

$$y = \alpha + f_1(x_1) + f_2(x_2) + \dots + f_i(x_i) + \epsilon, \quad (1)$$

where $f_i(\cdot)$ are transfer functions [24]:

$$f_i(x_i) = \boldsymbol{\beta}_i^\top \cdot \mathbf{b}_i(x_i), \quad (2)$$

$\boldsymbol{\beta}_i$ is a vector of model weights and $\mathbf{b}_i(\cdot)$ is a vector of polynomial basis functions, typically depending on one or two continuous variables in the vector of covariates \mathbf{x} . The GAM models are characterized by the number of basis functions used for each feature and the corresponding polynomial order. In addition, the regularisation parameter λ penalizes the convexity of the model in the fitting procedure.

An RF is an ensemble of decision trees “grown” from a subset of the training data. Each new training set is drawn, with replacement, from the original training set. Then a decision tree with fixed predefined maximal depth is grown from the new training set by randomly selecting a certain number of features [25]. The ensemble produces B outputs $\{\hat{y}_i = T_1(x), \hat{y}_2 = T_2(x), \dots, \hat{y}_B = T_B(x)\}$ where $\hat{y}_b, b = 1, \dots, B$ is the prediction for SST by the b^{th} decision tree. Outputs of all trees are averaged to predict \hat{y} [26]. Some of the key advantages of RFs are efficiency (easily parallelised), robustness to outliers and noise, and insight to feature importance [27] during model interpretation.

XGBoost shares many characteristics with RFs with a key difference being that decision trees are built *sequentially* rather than *independently*. In this manner, subsequent decision trees are built to further minimise prediction residuals. Prediction is of the form [28]:

$$\hat{y}_i = \phi(x_i) = \sum_{k=1}^K f_k(x_i), \quad f_k \in \mathcal{F}, \quad (3)$$

where $\mathcal{F} = \{f(x) = w_{q(x)}\}$ represent classification and regression trees, q represents each independent decision-tree structure, and w are leaf weights. \mathcal{F} is computed by minimising the objective function [28]:

$$\begin{aligned} \mathcal{L}_\phi &= \sum_i l(\hat{y}_i, y_i) + \sum_k \Omega(f_k), \\ \text{with } \Omega(f) &= \frac{1}{2} \lambda \|w\|^2, \end{aligned} \quad (4)$$

with l being a differentiable convex loss function (for example the mean squared error) of the difference between the prediction \hat{y}_i and the observation y_i for each T . The regularisation term, Ω , smooths the final weights

to avoid over-fitting (λ is a regularisation coefficient). Furthermore, a restriction to a maximal tree depth serves to regulate model complexity.

Gradient boosting of (4) proceeds in an additive manner to minimise the objective:

$$\mathcal{L} = \sum_i^n l(y_i, \hat{y}_i^{t-1} + f_t(x_i)) + \Omega(f_t). \quad (5)$$

The fundamental approach identifies f_t that most improves the prediction according to (4).

The first DL-based approach investigated was an MLP model. A MLP solves an optimisation problem to compute the weights and biases that represent the nonlinear function mapping inputs to the best representation of outputs, $\hat{\mathbf{y}}$:

$$g(\mathbf{X}; \Theta) = \hat{\mathbf{y}}. \quad (6)$$

Θ denotes the mapping matrix of weights and biases that represents the relationship between SST and explanatory variables, \mathbf{X} in the form of a neural network at each time point. During training, where the network is presented with a vector of observations, \mathbf{y} , an optimization problem is solved until the output of the network's last layer consistently approximates the training data set [29]. To counteract overfitting, L2-regularisation is used to penalise very large network weights. Regularisation is controlled by a user-defined parameter λ .

Cognizant of the temporal nature of the data, we investigated the performance of recurrent neural network (RNN) type models. A fundamental extension of RNNs compared to artificial neural networks is parameter sharing across different parts of the model. This has natural applicability to the forecasting of time-series variables with historical dependency as in this paper. An RNN with a single cell recursively computes the hidden vector sequence \mathbf{h} and output vector sequence \mathbf{y} iteratively from $t = 1, \dots, T$ in the form [30]:

$$\begin{aligned} h_t &= \mathcal{H}(W_{xh}x_t + W_{hh}h_{t-1} + b_h), \\ y_t &= W_{hy}h_t + b_y. \end{aligned} \quad (7)$$

where the \mathbf{W} terms denote weight matrices (e.g. \mathbf{W}_{xh} is the input-hidden weight matrix), the \mathbf{b} terms denote bias vectors (e.g. \mathbf{b}_h is hidden bias vector) and \mathcal{H} is the hidden layer function which is typically implemented as a sigmoid function. In effect, the RNN has two inputs, the present state and the past.

Standard RNN approaches have been shown to fail when lags between response and explanatory variables exceed 5–10 discrete timesteps [31]. Repeated applications of the same parameters can give rise to vanishing, or exploding gradients leading to model stagnation or

instability [29]. A number of approaches have been proposed in the literature to address this, with the most popular being LSTM.

Instead of a simple weighted dependency, 'LSTM cells' also have an internal recurrence (a self-loop), that serves to guide the flow of information and reduce susceptibility to vanishing or exploding gradients. Each cell has the same inputs and outputs as an ordinary recurrent network, but also has more parameters and a system of gating units that controls the flow of information. An LSTM model has a number of gates: input, output and forget gates that decide whether to let information in, forget information because it is not important, or let it impact output at the current timestep, respectively. As new input comes in, its impact can be accumulated to the cell, forgotten or propagated to the final state depending on the activation of the relevant gates [32]. In analogy to the MLP, we use L2-regularisation of weights represented by the parameter λ . More details on LSTM are provided in [31].

3.2. Feature Engineering

In data-driven modelling, judicious feature engineering facilitates expedited convergence to a solution. Automated feature selection improves predictive skills while allowing for greater transportability to other geographical locations where the characteristics of explanatory variables may vary. Figure 1 shows multi-year SST data illustrating primary trends. A monthly rolling mean of the data (middle plot) was subtracted from the raw data (top plot) with residuals presented (bottom plot). The long-term seasonal trend of the data is evident with yearly trends capturing a significant portion of the data variance. The data residuals largely represent short-term fluctuations in the data (together with sensor uncertainty component). The objective of the modelling was to learn the nonlinear relationships between the explanatory variables and the long- and short-term trends of the data.

The feature variables used for this study consisted of SST historical time series from MODIS and atmospheric data from TWC. From these data, several different types of input features were designed. Due to seasonal trends in the data, time features were included, i. e., year, month, week and season. Auto-regressive (AR) features quantified the influence of the recent past from the previous day up to a specified maximum number of daily lags (i.e. specifying a daily lag n , then to predict SST at time $t + 1$, SST from time $t - n$ to t were included as explanatory features). To predict multiple days in advance, AR features consisted of prediction from the previous model in an iterative manner – this allowed for long-term prediction

but introduced the possibility of systematic model error and bias (i. e., prediction error accumulated).

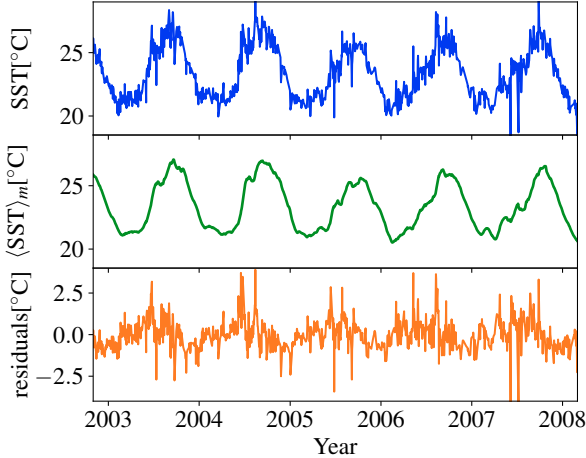


Figure 1: SST time series from MODIS measurements (upper panel), monthly rolling mean (middle panel), and residuals after subtraction of the monthly rolling mean from the SST data (lower panel).

TWC atmospheric data consisted of 18 time-dependent atmospheric quantities, including air temperature, solar radiation flux, cloud cover and winds [33]. As a first estimate, all atmospheric quantities at the desired time were considered and the model decided between the impact of each on the prediction during training (named TWC1). To reduce the number of covariates (and hence network size and associated demands for training data), a feature-selection module quantified the most important variables. Univariate feature selection was performed by computing F -scores from the correlation of each single features with the output label [34] and retaining the three atmospheric features with highest scores (TWC2). This concept can be further extended with time-dependent information by assigning univariate scores to lagged values of selected features and choosing the lags with the highest scores as features (TWC3).

3.3. Model Scoring and Aggregation

To assess the different modelling approaches, hyperparameters, and combinations of input features, the time series was split into training (90%) and test (10%) sets. The models were trained to make a prediction one day ahead based on feeding the previously described features and labels (measured value of SST for that day). The test datasets were then used to evaluate the performance of the model prediction against measured values.

As prediction depended on historic estimates of SST (i.e. a prediction for one day ahead required information

on the current SST), the model prediction was fed back as a feature to the model in a recurrent fashion. Specifically, the first test prediction ($t = 1$) was made with *measured* values of SST (at time $t = 0$) as a feature. For future predictions, the measured SST feature was replaced with the *prediction* from the previous day, i.e. prediction at time $t = 2$ received as input feature, model prediction for time $t = 1$ instead of the satellite derived value of SST, which in practise would not be available for forecasting multiple days in advance. Scoring for the entire test dataset (562 days) proceeded in this manner. This made the study extremely sensitive to propagation of error, where a low skill prediction propagates through the entire forecasting period.

The mean average error (MAE) and mean absolute percentage error (MAPE) assessed the accuracy of each model:

$$\text{MAE} = \frac{1}{N_{\text{test}}} \sum_{i=1}^{N_{\text{test}}} |(y - \hat{y})|, \quad \text{MAPE} = \frac{100}{N_{\text{test}}} \sum_{i=1}^{N_{\text{test}}} \left| \frac{(y - \hat{y})}{y} \right|, \quad (8)$$

where N_{test} is the size of the training data, y is the measured data, and \hat{y} the model-predicted equivalent. Finally, the models were aggregated into a single best prediction weighted by the inverse MAPE of the test data [35].

4. Model training and evaluation

Initial model training and testing was conducted on an arbitrary location in the North Atlantic: ($27^{\circ}28'46.45''$ N, $32^{\circ}25'43.71''$ W) – this focused on optimising the feature selection and hyperparameter tuning components. The models were then evaluated on a set of 730 points distributed globally. The accuracy of predictions generated at the evaluation stage were compared to state-of-the-art forecasts from the ECMWF numerical model.

Satellite measurements from MODIS spectrometer were collected over 16 years from July 2002 to December 2018. Due to measurement restrictions, (e. g., cloud cover interference) only 43% of that period had valid data. As data gaps are problematic for the training of time-series models (due to auto regressive features), linear interpolation between adjacent values replaced the missing data. Experiments revealed that the approach to missing-data handling had no significant impact on results. Moreover, the secondary weather input, TWC reanalysis data, were complete. During model validation, MAE and MAPE metrics were computed against the non-interpolated values to avoid potential contamination of the performance scores by the linear interpolation.

Model	Hyperparameters
GAM	# of splines/features $\in \{10, 15, 20\}$ polynomial-spline order $\in \{3, 5, 8\}$ $\lambda \in \{0.001, 0.01, 0.1, 1, 10, 100\}$
RF	# of trees/features $\in \{100, 200, 500\}$ max # of features $\in \{3, 5, 10\}$ max depth $\in \{5, 10, 15, 20\}$
XGBoost	# of trees/features $\in \{500, 700, 1000\}$ max depth $\in \{5, 10, 15, 20\}$ $\lambda \in \{0.01, 0.05, 0.1, 0.5\}$
MLP	# of layers $\in \{5, 10, 20\}$ # of nodes/layer $\in \{20, 50, 75\}$ $\lambda \in \{0.001, 0.01, 0.1, 1\}$
LSTM	# of layers $\in \{1, 2\}$ # of units/layer $\in \{1, 2, 3\}$ $\lambda \in \{0.001, 0.01, 0.1, 1\}$

Table 1: Hyperparameters and ranges used for model design. See Section 3.1 for details on each model hyperparameter

Optimising model performance included both parameter and feature selection. Hyperparameter optimisations adopted a greedy, grid-search approach over the user-defined parameter ranges summarised in Table 4. The 10% test-data size provided a sample size of over 18 months allowing assessment of different seasonal trends over the prediction period. (total data length was 16 years).

As previously described, the experiments compared a number of feature selection approaches to incorporate atmospheric and autoregressive effects. Initially AR features were manually selected based on heuristic information. For the GAM, RF and XGBoost models, the lags were restricted to the preceding 30 days, which balanced computational tractability with predictive skill. To incorporate seasonal effects (and also due to greater computational efficiency), the MLP and LSTM model were fed data from up to the previous 400 days (to extend beyond one year of historical trend). The experiments were set up by skipping the first 400 days to ensure meaningful AR features followed by splitting the data into training and test sets (last 18 months of data constituted the test set). Hyperparameter optimisation and feature selection proceeded iteratively for each model. For all features sets investigated, a full grid search of hyperparameters converged on the optimal combination of features and topology.

A more detailed feature selection module considered other combination of inputs, including: temporal infor-

mation (season, month, week), moving-window time-series fractions of the SST series (AR features), all available TWC atmospheric variables (TWC1), TWC variables extracted by univariate selection (TWC2), and lagged TWC variables selected by univariate tests (TWC3). Table 4 presents model-selection results considering hyperparameters and feature engineering. AR features provided adequate predictive skill for short-term forecasting (up to two days). For long-term predictions, atmospheric feature were critical for performance. The combination of model complexity and size of the features datasets are evident. Relatively simple models like GAM and RF provided best performance with more sophisticated feature engineering that reduced the size of the dataset. However, MLP and XGBoost both yielded the lowest test MAPE when provided with the full atmospheric dataset and allowed to infer relationships from all variables and data labels.

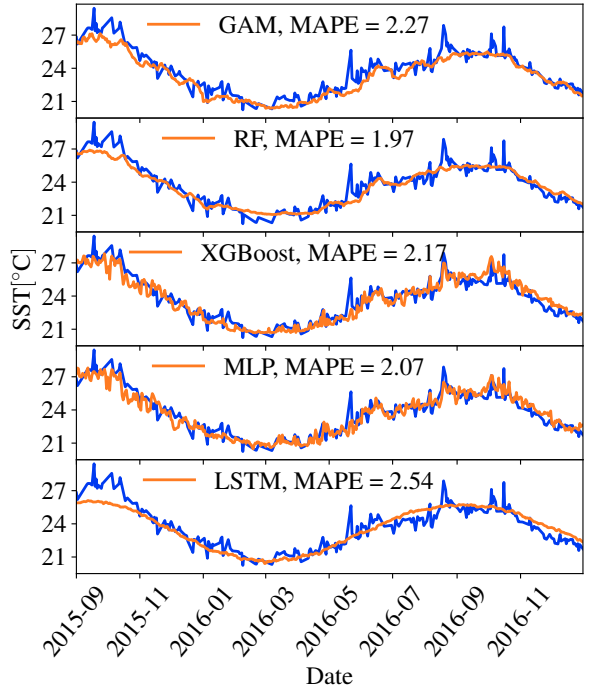


Figure 2: Test-prediction (orange curve) of SST at $27^{\circ}28'46.45''$ N, $-32^{\circ}25'43.71''$ W from different ML models trained on 12 years of preceding historical data compared to measured SSTs (blue curve). Feature combinations and hyperparameters adopted for each model are summarised in Table 4.

In addition to MAPE accuracy, Table 4 also lists the run times needed to train the corresponding models (on a commodity laptop). Training times were within acceptable limits for all models, although significant variability existed. As expected, the LSTM had the largest com-

putational demand. However, it also had the highest MAPE. This non-intuitive result demonstrates the need to balance model complexity with the nature of the data. That is, naïve selection might suggest that an RNN-based model such as LSTM is most suitable for a time-series dataset. However, results demonstrated that the LSTM model failed to capture the high-frequency variations in the data despite replicating seasonal trends (the monthly rolling-mean trends reported in Figure 1) quite well. This is due to the “long memory” for this model that interfered with learning short-term variations. In contrast, simpler models with time-series information explicitly included as features better learned short-term dynamics.

Figure 2 compares model predictions (see Table 4) for the test period to MODIS data. Observing the time evolution of SST reveals that a suitable model must represent two distinct time scale components. On the one hand there is the smooth SST evolution governed by seasonality. This component of SST evolution benefited from suppression of large fluctuations. Of the models studied, this criterion was fulfilled by the GAM approach, which yielded lowest test MAPE with a large regularization parameter $\lambda = 10$ (i.e., the penalty on the second-order derivative of fitted single-feature functions). The large regularization effect together with the piecewise polynomial components of GAM models contributed to a smoother time-series prediction that still captured long-term trends, including correlation of data between years. Similarly, the RF approach led to a comparably smooth SST evolution but at significantly lower MAPE than the GAM model. The most obvious reflection of the seasonal trend is evident in the LSTM prediction which produces a highly smoothed representation of the training data. The model fails to capture any small-scale dynamics at the daily or weekly level instead reproducing the seasonal heating/cooling effects only. Further analysis of model parameters suggested this to be a result of the retained long-term memory informing the broader trend only. On the other hand, the seasonal cycle has superimposed on it short-term behaviour dominated by peak events occurring at daily to weekly time scales. This is particularly evident in the XGBoost and the MLP approaches where both yielded best performances for smaller λ , which enabled them to better capture short-term events. It’s worth noting that while XGBoost and MLP captured the small-scale fluctuations better, RF returned lowest MAPE. To simultaneously take both aspects into account, a model combination weighted by the inverse MAPE can better represent observed dynamics [35]. As a preprocessing step, due to the comparably poor performance of the LSTM model, it was excluded from the ensemble.

4.1. Transportability and Comparison to State-of-the-art

As the feature engineering and hyperparameter selection process is complex, it is desirable to execute this procedure once and then use the selected model at different locations. We investigated the performance of the model at 730 globally distributed locations. Data (SST measurements and TWC weather variables) were collected in a $6^\circ \times 6^\circ$ grid of points within 1° of shorelines between $\pm 54^\circ$ latitude. Again using a 90%/10% train and test data split, we trained each of the models using the hyperparameters noted in Table 4. The resulting prediction was again an aggregation of GAM, RF, XGBoost, and MLP results, where each model was weighted by the inverse MAPE at each location to favour models with better performance in the weighted average. Figure 3 presents the MAE and MAPE computed at these 730 locations. Results demonstrate that MAE and MAPE were less than 1°C and 10%, respectively, at most locations. Table 4.1 presents average error metrics over all locations. The MAPE-weighted ensemble average returned MAE and MAPE of 0.68°C and 7.9% respectively. These values are comparable to ECMWF estimates on SST which returned values of 0.56°C and 12.3%, respectively. While ECMWF reports lower absolute error, relative errors are noticeably higher. This suggests a tendency of the numerical outputs to perform poorer in periods when temperatures are lower (increasing relative error).

Figure 3 indicates some spatial variations in performance. MAPE is understandably higher in southern and northern latitudes where mean temperatures are lower and relative differences more pronounced. There is a slight trend towards higher MAE in near-coast locations, where oceanic processes can be more complex driven by secondary processes (e.g. upwelling and downwelling events). Across the globe however, the framework presents excellent predictive skill demonstrating a transportable approach to provide data-driven predictions of SST.

5. Results and Discussion

Time-series forecasts are vital in many areas of scientific, industrial, and economic activity. Many ML methods have been applied to such problems and the advantages of RNN-type approaches are well documented. The ability of these DL algorithms to implicitly include effects from preceding time steps is intuitively a natural fit. However, this study demonstrated that when the relationship between predicted values was not based

Model	Features	Hyperparameters	Training time [sec]	MAPE
GAM	TWC3, time	# of splines = 20, spline order = 8, $\lambda = 10$	1.67	2.27
RF	AR, TWC3, time	# of trees = 500, max # of features = 3, max depth = 20	19.09	1.97
XGBoost	TWC1, time	# of trees = 1,000, max depth = 5, $\lambda = 0.05$	0.21	2.17
MLP	TWC1, time	# of layers = 20, of units/layer = 20, $\lambda = 0.01$	11.18	2.07
LSTM	TWC2	# of layers = 1, # of units/layer = 2, $\lambda = 0.1$	71.67	2.54

Table 2: Model-selection result for the two North Atlantic locations.

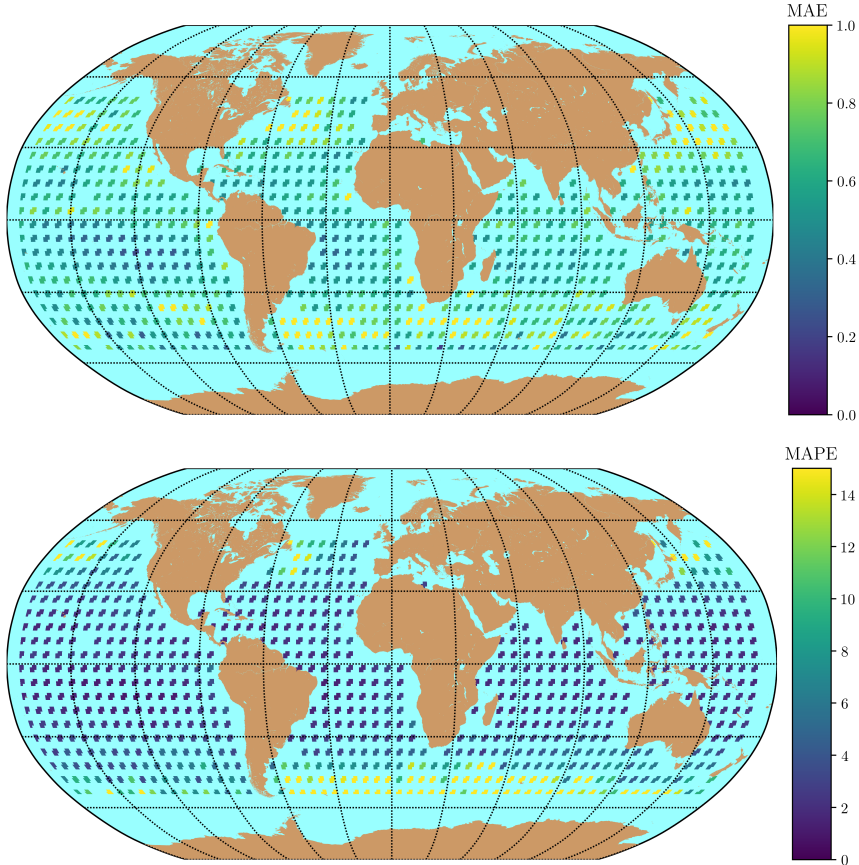


Figure 3: Predictive skill of a weighted ensemble average of GAM, RF, XGBoost, and MLP models at a set of locations distributed equally between $\pm 54^\circ$ latitude. MAE (top) and MAPE (bottom) metrics are presented to inform on absolute and relative errors. The model selection, used features and hyperparameters from the training experiments presented in Table 4.

Metric	GAM	RF	XGBoost	MLP	Ens. Ave.	ECMWF
MAE	0.78	0.72	0.79	0.89	0.68	0.56
MAPE	9.7	9.4	8.8	10.6	7.9	12.3

Table 3: MAE and MAPE averaged across all spatial locations presented in Figure 3. Metrics are presented for each model individually, an ensemble averaged weighted by the inverse MAPE and the final column presents error metrics for a benchmark ECMWF model against MODIS measurements.

solely on AR features – well-designed feature selection in conjunction with simpler ML methods capable to more rapidly adjust to short-scale fluctuations outperformed the DL approaches.

Table 4 demonstrated that the important features needed to predict at time $t + 1$ are SST values at time t (and values at earlier time steps dependent on selected AR features) and atmospheric information at time $t + 1$ (and potentially AR features of those). Hence, prediction required inclusion of AR features while inferring

relationships between forecasted values of atmospheric data and the response variable, SST. Figure 2 illustrated that the LSTM model failed to adequately learn the relationship between explanatory variables and SST. Specifically, the model closely approximated seasonal trends (i. e., the long-term characteristics of the SST) while failing to capture high-frequency variations (i. e., variations in response to atmospheric inputs). In effect, the DL approach maintained “memory” of the long-term SST trends to the detriment of incorporating effects of shorter time scales. A more focused feature-engineering module that guided the data-length fed to the LSTM model may improve performance. However, this contravenes the purpose of RNN-type approaches that aims to implicitly learn the nature of cyclic data. Another point worth noting is that DL approaches have a larger appetite for training data than some of the simpler models adopted. Some reduction in MAPE may be possible by extending the size of the training data. Again, however, when evaluating different modelling approaches, aspects such as computational complexity and ability to learn on smaller datasets are key points that demand consideration (further, there are practical limits on available data).

This study considered a framework to develop a transportable model suite applied to a nonlinear, real-world dataset. Key points considered were design of an automatic feature-engineering module, which, together with a standard hyperparameter optimisation routine, facilitated ready deployment at disparate geographical locations. Results demonstrated that the different models adopted had inherent characteristics that governed accuracy and level of regularization or overfit to training data.

We compared performance of ML models with a state-of-the-art physics-based approach from ECMWF. As expected, the physics-based model yielded low MAPE against satellite measurements – the ECMWF prediction is a reanalysis product which assimilates measurement (including satellite) data daily to update the accuracy of the product. This study demonstrated, however, that the machine learning based approaches achieve accuracy comparable to ECMWF model, at a fraction of the computational expense. Aggregating the models improved the robustness of this approach and served to regularize small-scale fluctuations or seasonal biases in individual models. Figure 4 compares the ensemble predictions to the ECMWF results, satellite measured SST and predictions from the best performing ML model (RF) at an arbitrary location ($36^{\circ}12'58.8''$ N, $61^{\circ}14'1.24''$ W). The best performing model (RF) provides good predictive skill comparable to ECMWF, while the aggregated

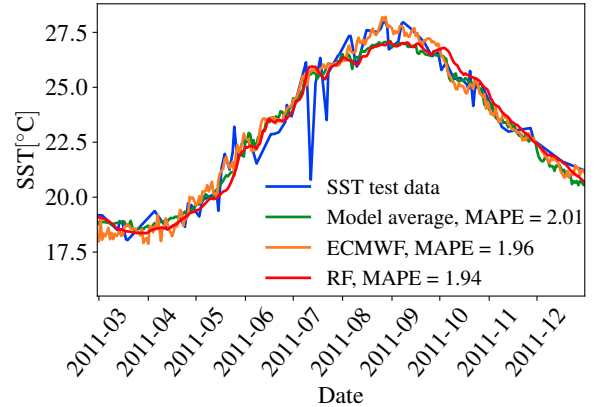


Figure 4: Weighted ensemble average of GAM, RF, XGBoost, and MLP models at $36^{\circ}21'58.8''$ N, $61^{\circ}14'1.24''$ W compared to a state-of-the-art physics-based ocean model (ECMWF), best performing independent model (RF) and the measured SST. Prescribed features and parameters are described in Table 4

model is ‘smoother’ (possibly more robust to short-scale fluctuations), while achieving comparable accuracy.

Classical works on ensemble forecasting demonstrated that the ensemble mean should give a better forecast than a single deterministic forecast [36, 37]. Assigning inverse MAPE weights to individual models provides a simple and effective method to rank model contributions based on performance. Interrogating temporal evolution of model error over the 18-month test period demonstrated some biases in individual models e.g. GAM outperformed RF during the summer period but is significantly poorer during periods of lower temperature. The ensemble aggregation framework we implemented reduced error over the duration of the test period compared to arbitrarily selected individual models, but more importantly, also served to reduce error and biases at distinct periods of the prediction window. Table 5 presents MSE against satellite data for each individual model and the ensemble aggregation over the duration of the study period at the same location as Figure 4.

Season	GAM	RF	XGBoost	MLP	Ens. Ave.
Spring	1.37	1.04	1.01	0.90	0.94
Summer	0.18	0.40	0.45	0.68	0.30
Autumn	0.06	0.10	0.40	0.80	0.17
Winter	0.26	0.14	0.39	0.34	0.22

Table 4: Seasonal MSE for individual models and ensemble average

The envisioned applications of this approach are for 1) long-term climatological based approaches where the

framework can be used to compute response to related trends or 2) short-term, operational type forecasting where 5-10 day forecasts are computed and used to inform particular decision. Within these scenarios there are likely differences in how the ML models are integrated into this system rather than differences in the ML models themselves. In particular, short-term prediction could be improved by combining individual models using aggregation techniques that weighs models more heavily based on predictive skill in the recent past (e.g. [38]). Long-term, climatology-type predictive studies, on the other hand are often used in conjunction with stochastic inputs and system response based on probabilistic analysis.

This study presented a robust time-series forecasting framework applied to satellite measurement of SST. We considered the SST data as a set of disparate points. In reality, the ocean surface more closely resembles an image with interaction between points (or pixels). Results demonstrated that treating the data as distinct time-series points provided good results. However, scope exists to combine this approach with image-processing techniques such as convolutional neural networks (CNNs) to incorporate neighbouring effects into predictions. Future work will explore the viability and value of combining CNNs with time-series forecasting models to further improve the robustness of the framework.

6. Conclusions

This paper demonstrates the viability of applying ML based approaches, addressing transportability, biases and robustness by combining feature selection and disparate models with specific characteristics in a weighted aggregation based on average model performance. This study aimed to assess the ability of data-driven approaches to accurately predict SST characterised by seasonal trends, temporal dependencies and short-term fluctuations. Results demonstrate comparable performance to physics-based model simulations with low computational cost, and which is easily parametrised to other geographical locations. The low computational cost of the approach has many advantages. First, it enables separation of SST forecasting models from HPC centres – the suite of models presented here can be trained on a laptop and applied to any geographic location. Once trained, the inference step is of negligible computational expense and can be readily deployed on edge-type devices (e.g. in-situ devices deployed in the ocean). Deploying large-scale models is a complex task highly dependent on user skill to correctly configure and parametrise to specific

locations. Data-driven approaches can present an alternative approach that enables rapid prediction, contingent on availability of sufficient data.

Acknowledgements

This project has received funding from the European Unions Horizon 2020 research and innovation programme as part of the RIA GAIN project under grant agreement No. 773330.

References

References

- [1] S. O. Handeland, A. K. Imsland, S. O. Stefansson, The effect of temperature and fish size on growth, feed intake, food conversion efficiency and stomach evacuation rate of Atlantic salmon post-smolts, *Aquaculture* 283 (1-4) (2008) 36–42.
- [2] S.-J. Huang, J.-T. Lin, Y.-T. Lo, N.-J. Kuo, C.-R. Ho, The coastal sea surface temperature changes near the nuclear power plants of northern Taiwan observed from satellite images, in: *OCEANS 2014 - TAIPEI*, IEEE, 2014, pp. 1–5.
- [3] R. E. Davis, Predictability of Sea Surface Temperature and Sea Level Pressure Anomalies over the North Pacific Ocean, *Journal of Physical Oceanography* 6 (3) (1976) 249–266.
- [4] S. Hirahara, M. A. Balmaseda, E. De Boisseson, H. Hersbach, 26 Sea Surface Temperature and Sea Ice Concentration for ERA5, Tech. rep., Reading, UK (2016).
- [5] M. Bell, A. Schiller, P.-Y. Le Traon, N. Smith, E. Dombrowsky, K. Wilmer-Becker, An introduction to GODAE OceanView, *Journal of Operational Oceanography* 8 (sup1) (2015) s2–s11.
- [6] F. Rawlins, S. Ballard, K. Bovis, A. Clayton, D. Li, G. Inverarity, A. Lorenc, T. Payne, The met office global four-dimensional variational data assimilation scheme, *Quarterly Journal of the Royal Meteorological Society* 133 (623) (2007) 347–362.
- [7] M. Martin, M. Balmaseda, L. Bertino, P. Brasseur, G. Brassington, J. Cummings, Y. Fujii, D. Lea, J.-M. Lellouche, K. Mogensen, P. Oke, G. Smith, C.-E. Testut, G. Waagbø, J. Waters, A. Weaver, Status and future of data assimilation in operational oceanography, *Journal of Operational Oceanography* 8 (sup1) (2015) s28–s48.
- [8] E. J. O’Dea, A. K. Arnold, K. P. Edwards, R. Furner, P. Hyder, M. J. Martin, J. R. Siddorn, D. Storkey, J. While, J. T. Holt, H. Liu, An operational ocean forecast system incorporating NEMO and SST data assimilation for the tidally driven European North-West shelf, *Journal of Operational Oceanography* 5 (1) (2012) 3–17.
- [9] S. Saha, S. Moorthi, X. Wu, J. Wang, S. Nadiga, P. Tripp, D. Behringer, Y.-T. Hou, H.-y. Chuang, M. Iredell, M. Ek, J. Meng, R. Yang, M. P. Mendez, H. van den Dool, Q. Zhang, W. Wang, M. Chen, E. Becker, S. Saha, S. Moorthi, X. Wu, J. Wang, S. Nadiga, P. Tripp, D. Behringer, Y.-T. Hou, H.-y. Chuang, M. Iredell, M. Ek, J. Meng, R. Yang, M. P. Mendez, H. van den Dool, Q. Zhang, W. Wang, M. Chen, E. Becker, The NCEP Climate Forecast System Version 2, *Journal of Climate* 27 (6) (2014) 2185–2208.
- [10] E. Chassignet, H. Hurlburt, E. J. Metzger, O. Smedstad, J. Cummings, G. Halliwell, R. Bleck, R. Baraille, A. Wallcraft, C. Lozano, H. Tolman, A. Srinivasan, S. Hankin, P. Cornillon, R. Weisberg, A. Barth, R. He, F. Werner, J. Wilkin, US GODAE:

Global Ocean Prediction with the HYbrid Coordinate Ocean Model (HYCOM), *Oceanography* 22 (2) (2009) 64–75.

[11] Y. Chao, Z. Li, J. Farrara, J. C. McWilliams, J. Bellingham, X. Capet, F. Chavez, J.-K. Choi, R. Davis, J. Doyle, P. Li, P. Marchesiello, M. A. Moline, J. Paduan, S. Ramp, Development, implementation and evaluation of a data-assimilative ocean forecasting system off the central California coast, *Deep Sea Research Part II: Topical Studies in Oceanography* 56 (3-5) (2009) 100–126.

[12] D. B. Haidvogel, H. Arango, W. P. Budgell, B. D. Cornuelle, E. Curchitser, E. Di Lorenzo, K. Fennel, W. R. Geyer, A. J. Hermann, L. Lanerolle, Others, Ocean forecasting in terrain-following coordinates: Formulation and skill assessment of the Regional Ocean Modeling System, *Journal of Computational Physics* 227 (7) (2008) 3595–3624.

[13] E. de Bezenac, A. Pajot, P. Gallinari, Deep Learning for Physical Processes: Incorporating Prior Scientific Knowledge, *arxiv preprint arXiv:1711.07970arXiv:1711.07970*.

[14] S. Wiewel, M. Becher, N. Thuerey, Latent-space Physics: Towards Learning the Temporal Evolution of Fluid Flow, *arxiv preprint arXiv:1802.10123arXiv:1802.10123*.

[15] D. J. Lary, A. H. Alavi, A. H. Gandomi, A. L. Walker, Machine learning in geosciences and remote sensing, *Geoscience Frontiers* 7 (1) (2016) 3–10.

[16] S. C. James, Y. Zhang, F. O’Donncha, A machine learning framework to forecast wave conditions, *Coastal Engineering* 137 (2018) 1–10.

[17] P. M. R. DeVries, T. B. Thompson, B. J. Meade, Enabling large-scale viscoelastic calculations via neural network acceleration, *Geophysical Research Letters* 44 (6) (2017) 2662–2669.

[18] E. Arandia, F. O’Donncha, S. McKenna, S. Tirupathi, E. Ragnoli, Surrogate modeling and risk-based analysis for solute transport simulations, *Stochastic Environmental Research and Risk Assessment* (2018) 1–15.

[19] J. Li, A. D. Heap, A. Potter, J. J. Daniell, Application of machine learning methods to spatial interpolation of environmental variables, *Environmental Modelling & Software* 26 (12) (2011) 1647–1659.

[20] A. Ducournau, R. Fablet, Deep learning for ocean remote sensing: an application of convolutional neural networks for super-resolution on satellite-derived SST data, in: 2016 9th IAPR Workshop on Pattern Recognition in Remote Sensing (PRRS), IEEE, 2016, pp. 1–6.

[21] B. Gokaraju, S. S. Durbha, R. L. King, N. H. Younan, A Machine Learning Based Spatio-Temporal Data Mining Approach for Detection of Harmful Algal Blooms in the Gulf of Mexico, *IEEE Journal of Selected Topics in Applied Earth Observations and Remote Sensing* 4 (3) (2011) 710–720.

[22] K. Kilpatrick, G. Podestá, S. Walsh, E. Williams, V. Halliwell, M. Szczodrak, O. Brown, P. Minnett, R. Evans, A decade of sea surface temperature from MODIS, *Remote Sensing of Environment* 165 (2015) 27–41.

[23] T. J. Hastie, R. J. Tibshirani, *Generalized Additive Models.*, CRC Press, 1990.

[24] T. K. Wijaya, M. Sinn, B. Chen, Forecasting Uncertainty in Electricity Demand, in: Workshops at the Twenty-Ninth AAAI Conference on Artificial Intelligence, 2015.

[25] L. Breiman, Random Forests, *Machine Learning* 45 (1) (2001) 5–32.

[26] V. Svetnik, A. Liaw, C. Tong, J. C. Culberson, R. P. Sheridan, B. P. Feuston, Random forest: a classification and regression tool for compound classification and qsar modeling, *Journal of chemical information and computer sciences* 43 (6) (2003) 1947–1958.

[27] G. Louppe, L. Wehenkel, A. Sutera, P. Geurts, Understanding variable importances in forests of randomized trees, in: *Advances in neural information processing systems*, 2013, pp. 431–439.

[28] T. Chen, C. Guestrin, XGBoost, in: *Proceedings of the 22nd ACM SIGKDD International Conference on Knowledge Discovery and Data Mining - KDD ’16*, ACM Press, New York, New York, USA, 2016, pp. 785–794.

[29] I. Goodfellow, Y. Bengio, A. Courville, *Deep learning*, 2015.

[30] A. Graves, A.-r. Mohamed, G. Hinton, Speech recognition with deep recurrent neural networks, in: *2013 IEEE International Conference on Acoustics, Speech and Signal Processing*, IEEE, 2013, pp. 6645–6649.

[31] F. Gers, Learning to forget: continual prediction with LSTM, in: *9th International Conference on Artificial Neural Networks: ICANN ’99*, Vol. 1999, IEE, 1999, pp. 850–855.

[32] X. Shi, Z. Chen, H. Wang, D.-Y. Yeung, W.-k. Wong, W.-c. WOO, Convolutional LSTM Network: A Machine Learning Approach for Precipitation Nowcasting (2015).

[33] IBM, Weather Company Data API, Tech. rep., The Weather Company (2018).

[34] I. Guyon, S. Gunn, M. Nikravesh, L. A. Zadeh, *Feature extraction: foundations and applications*, Vol. 207, Springer, 2008.

[35] R. Adhikari, R. K. Agrawal, Combining multiple time series models through a robust weighted mechanism, in: *2012 1st International Conference on Recent Advances in Information Technology (RAIT)*, 2012, pp. 455–460.

[36] E. S. Epstein, Stochastic dynamic prediction, *Tellus* 21 (6) (1969) 739–759.

[37] C. Leith, Theoretical skill of monte carlo forecasts, *Monthly Weather Review* 102 (6) (1974) 409–418.

[38] F. O’Donncha, Y. Zhang, B. Chen, S. C. James, An integrated framework that combines machine learning and numerical models to improve wave-condition forecasts, *Journal of Marine Systems* 186 (2018) 29–36.